https://doi.org/10.5194/egusphere-2025-190
Preprint. Discussion started: 7 March 2025


# Isotopic evidence for the impact of artificial snow on the nitrogen cycle in temperate regions

Hyejung Jung[1], Yalalt Nyamgerel[1], Kyung-Seok Ko[2], Dong-Chan Koh[2], Weon-Seo Kee[2], Jeonghoon Lee[1*]

[1]Department of Science Education, Ewha Womans University, Seoul 03760, Korea
[2]Korea Institute of Geoscience and Mineral Resources, Daejeon 34132, Korea

*Correspondence to*: Jeonghoon Lee (jeonghoon.d.lee@gmail.com)

**Abstract.** As winters become warmer due to climate change, ski resorts around the world are increasingly and preferentially relying on artificial snow instead of natural snow. The chemical species contained in artificial snow can flow into the surrounding hydrological system along with melted snow, resulting in unexpected environmental pollution. This study is the first attempt to assess the impact of artificial snow on groundwater quality and its role in the nitrogen (N) cycle. Although numerous multi-isotope approaches exist for identifying sources and estimating the contributions to nitrate pollution, few studies have used nitrogen isotopes of nitrate ($\delta^{15}N–NO_3^-$) and oxygen isotopes of water ($\delta^{18}O–H_2O$) simultaneously as tracers. This study aimed to evaluate the impact of artificial snow on the quality of surrounding groundwater at a ski resort, located in Mt. Balwang in Pyeongchang, South Korea (the 2018 Winter Olympics venue). Mt. Balwang, located in the upstream region of the Han River, is a critical source of water that joins major tributaries forming the upper Han River, which supplies drinking water to over 25 million residents in the metropolitan Seoul area. The average N contribution of mountain groundwater estimated using Bayesian mixing models was the highest from artificial snow (49.5%), originating from manure and sewage, exceeding rainfall (31.6%) and natural snow (18.7%). These results are closely consistent with theoretical N loading rates, highlighting the potential for artificial snow to contribute to long-term N accumulation in alpine ecosystems. Our study highlights the importance of continuous monitoring to mitigate potential disruptions to the N cycle and preserve ecosystem stability as climate change increases dependence on artificial snow.

## 1 Introduction

Human activities are altering the global N cycle through anthropogenic N inputs, including the production of combustion of fossil fuel use, N fertilizers, and cultivation of N-fixing crops (Galloway et al., 1995; Erisman et al., 2013). Over the past 50 to 100 years, these activities have increased the global anthropogenic rate of $N_2$ fixation, which is currently estimated to be approximately 1.5 to 2 times higher than the natural rate of $N_2$ fixation in terrestrial ecosystems (Galloway et al., 2003; Schlesinger, 2009). Supporters of ski tourism often argue that the water used for snowmaking is merely "borrowed" and eventually returns to mountain creeks and rivers during snowmelt (Morin et al., 2023). However, the impact of N in artificial snow on the surrounding alpine water systems has not yet been comprehensively addressed in the world.

https://doi.org/10.5194/egusphere-2025-190
Preprint. Discussion started: 7 March 2025


Snowmaking necessitates substantial energy as well as water consumption, a demand that is expected to escalate in proportion to the progression of warming trends by consuming fossil fules (Damm et al., 2014; Vorkauf et al., 2024; Knowles et al., 2024). Recent Winter Olympic Games in Sochi (2014; latitude 43° N), Pyeongchang (2018; latitude 37° N), and Beijing (2022; latitude 39° N) relied heavily on artificial snow, with Beijing's Yanqing site using almost 100% (IOC, 2022). Producing 1 $m^3$ of artificial snow requires approximately 200~500 liters of water, depending on humidity and air temperature (Rixen et al., 2013). This water consumption can impact local water availability in a warmer climate (Morin et al., 2023). According to Knowles et al. (2024), Canada presently utilizes 478,000 megawatts (MWh) of electricity, resulting in 130,095 tonnes of associated $CO_2$ emission, and 43.4 million $m^3$ of water to produce over 42 million $m^3$ of artificial snow. In particular, generating this electricity requires the use of fossil fuels, significant amounts of carbon dioxide ($CO_2$), a greenhouse gas, are emitted during the snowmaking process. The greenhouse gas emissions will exacerbate global warming, thereby fueling a cycle that further amplifies the need for artificial snow production. This feedback loop highlights a paradox where the activities intended to mitigate the effects of climate change in winter tourism may, in turn, contribute to the broader issue of global warming.

In this study, we evaluated the influence of artificial snow on surrounding groundwater quality in the water system in an alpine ski area of Yongpyong, South Korea, where the Pyeongchang Olympics were held in 2018 (Figure 1). Mt. Balwang, located in the upstream region of the Han River, is a critical source of water that joins major tributaries forming the upper Han River, which supplies drinking water to over 25 million residents in the metropolitan Seoul area. The ski resort, which opened in 1975, is famous as South Korea's first and largest ski resort, with an area of 1.10 million $m^2$. The ski slopes start at the summit of Mt. Balwang at a 1,458 m altitude and continue down to 700 m below the mountain. From the 2017/2018 season to the 2023/2024 season, the average annual volume of water used for snowmaking was 1.15 ± 0.15 million $m^3$. The water used for artificial snow production was sourced from the stream located at the entrance of the ski resort. Although mountain groundwater (W) wells were located in an area at the mountain summit without potential N pollutants, the average $NO_3^-$–N concentration is 4.0 ± 0.7 (1σ) mg/L (Table S1). This concentration was generally higher than 3 mg/L, which represents the natural (background) state, suggesting the presence of anthropogenic inputs (Madison and Brunett, 1985). As winter temperatures rise and extreme precipitation patterns become more frequent, the reliance on artificial snow is expected to increase over the past 22 years (2002–2023) at Yongpyong weather station in Korea (Figure 2).

Although numerous multi-isotope approaches exist for identifying sources and estimating the contributions to nitrate pollution, this study is the first attempt to simultaneously utilize nitrogen isotopes of nitrate ($\delta^{15}N$–$NO_3^-$) and oxygen isotopes of water ($\delta^{18}O$–$H_2O$) as tracers. The $\delta^{15}N$–$NO_3^-$ reveals the contamination sources, while the $\delta^{18}O$–$H_2O$ offers critical insights into the hydrological processes that affect the transport of nitrate pollutants, thereby increasing the precision of source tracking. The objectives of this study were (1) determine the origin of water and nitrogen (N) sources in mountain groundwater, (2) investigate the seasonal variation in N sources in mountain groundwater, and (3) evaluate the contribution of artificial snow to mountain groundwater. Based on this, we aim to gain new insight into the potential impacts of artificial snow on the N cycle.

https://doi.org/10.5194/egusphere-2025-190
Preprint. Discussion started: 7 March 2025


## 2 Methods

### 2.1 Sample collection and field measurements

We collected 63 samples from a ski resort located in Mt. Balwang and its surrounding areas from September 2020 to August 2022 (Figure 1). The geological features are detailed in Supplementary Information. Information related to snow sampling is presented in Table S2. Before taking snow samples, we measured the snow density and liquid water content (LWC) *in situ* using an SLF Snow Sensor (FPGA Company, Switzerland), and the sampling depth was determined based on these measurements. Artificial snow was collected at the ski resort at the mountain summit (1,458 m) on February 10, 2021. Artificial snow samples unaffected by natural snow were collected from two depths (50 cm and 75 cm) in February 2021. Natural snow that was not affected by artificial snow was collected twice on February 10, 2021, and March 2, 2021, at the mountain summit (Figure S1). Groundwater samples were collected from two wells (W1 and W2) at the mountain summit and from nine wells (YP1–YP9) at the bottom of the mountain. The groundwater wells W1 and W2 were developed at 300- and 350-m depths, respectively, on the mountain summit (1,458 m altitude) (Figure 1b). Meanwhile, groundwater wells (YP1–YP9) were also developed at various depths (23–400 m) under the mountain (700 m altitude).

The soil moisture content and soil temperature were measured with TEROS 12 (METER Group, Inc., United States) Frequency Domain Reflectometry (FDR) sensors, which were installed at three depths (8 cm, 18 cm, and 32.5 cm). Electrical conductivity (EC), temperature and pH were measured *in situ* using an Orion Star™ A329 pH/Conductivity multiparameter meter with a Thermo Scientific™ Orion™ Conductivity Probe and an Orion 8107UWMMD Ultra pH/ATC Triode. The EC probe was calibrated with 1413 μS $cm^{-1}$ standard solutions. The pH electrode was calibrated using pH = 4.01, 7.00, and 10.01 buffers. Samples for dissolved anions and total alkalinity ($A_T$), as well as those for water isotope and nitrate isotope measurements, were passed through 0.2-μm filters and collected in HDPE bottles. Dissolved cation samples underwent filtration through 0.2-μm filters and were subsequently acidified to pH = 2 utilizing concentrated, ultrapure $HNO_3$ before being gathered in HDPE bottles.

### 2.2 Chemical and isotope analysis

Anion concentrations were determined using an ion chromatograph (Dionex ICS-1500, Sunnyvale, CA, United States) equipped with an IonPac™ AS14 anion-exchange column at the Korea Institute of Geoscience and Mineral Resources (KIGAM). Cation concentrations were analyzed utilizing inductively coupled plasma-atomic emission spectrometry (Optima 7300DV, Perkin Elmer, Waltham, MA, United States) at the same institute. Total carbonate alkalinity in μeq/L ($A_T = HCO_3 + 2CO_3$) was quantified using the HACH Method 8203, adding Bromcresol Green-Methyl Red and Phenolphthalein indicator powder along with sulfuric acid (0.16 N). Charge balance error (CBE) indicates a discrepancy between the measured concentrations of cations (positively charged ions) and anions (negatively charged ions) in a sample solution. This is an indicator of the accuracy and reliability of quantitative results and is calculated using the formula CBE

https://doi.org/10.5194/egusphere-2025-190
Preprint. Discussion started: 7 March 2025


(%) = $(TZ^+ - TZ^-)/(TZ^+ + TZ^-) \times 100$, where $TZ^+ = 2Ca^{2+} + 2Mg^{2+} + K^+ + Na^+$ and $TZ^- = Cl^- + 2SO_4^{2-} + NO_3^- + A_T$. Typically, the average CBE is within ±10%.

Stable isotopic compositions of water ($\delta^{18}O$–$H_2O$ and $\delta^2H$–$H_2O$) were analyzed at Ewha Womans University (Seoul, Korea) using L2140-i isotopic water–liquid analyzer (Picarro Inc., Sunnyvale, CA, USA) through cavity ring-down spectroscopy (CRDS). CRDS involves passing a laser beam through a cavity containing the sample gas and measuring the rate of decay (ring-down) of the laser light intensity. The mean (± 1σ) accuracy and precision of the $\delta^{18}O$ and $\delta^2H$ contents for each sample were within ± 0.1‰ and ± 1.0‰, respectively. Stable isotopic compositions of nitrate ($\delta^{15}N$–$NO_3$ and $\delta^{18}O$–$NO_3$) were conducted at the Environmental Isotopes Lab at the University of Waterloo. Following conversion purified $NO_3^-$ to $NO_2^-$ through a cadmium catalyst then chemically reduced to $N_2O$ which is then analyzed on an Isoprime Trace Gas continuous flow mass spectrometer (GV Instruments Ltd., Manchester, UK). The mean (± 1σ) accuracy and precision of the $\delta^{18}O$ and $\delta^{15}N$ values for each sample were within ± 1.0‰ and ± 0.5‰, respectively.

All stable isotopic results were presented in delta notation (δ) in units per mil (‰) relative to the international reference standard, as described in Eq. (1):

$$\delta\ (‰) = \left\{\left(\frac{R_{\text{sample}}}{R_{\text{standard}}}\right) - 1\right\} \times 1000, \quad (1)$$

where R represents the ratio of heavy to light isotopes ($^2H/^1H$, $^{18}O/^{16}O$, or $^{15}N/^{14}N$), and $R_{sample}$ and $R_{standard}$ denote the isotopic ratios in the sample and standard, respectively. The ratios $^2H/^1H$ and $^{18}O/^{16}O$ are denoted as $\delta^2H$ and $\delta^{18}O$, respectively, relative to VSMOW, whereas the $^{15}N/^{14}N$ ratio of nitrate is represented as $\delta^{15}N$–$NO_3^-$ relative to atmospheric $N_2$.

### 2.3 Bayesian mixing models

Bayesian mixing models are statistical models used to estimate the proportions of different sources or components contributing to a mixture. Bayesian mixture models are useful for quantifying statistical probabilities that reflect uncertainty in estimating contributions from multiple potential sources (Parnell, 2008). The estimation of the N source proportion was carried out using stable isotope mixing models (SIMMs) in R (version 4.2.2). Among several R packages to conduct stable isotope mixing models, SIAR (Stable Isotope Analysis in R), which implements Bayesian mixing models was used. Three types of variables were utilized for the modeling: the isotopic ratio of mixtures, and the mean and standard deviation of the isotope ratio of the potential sources (Parnell and Inger, 2016). Additionally, an enrichment factor for the isotope can be added optionally (Parnell and Inger, 2016), although it was assumed to be 0 in this study. Isotope mixing analysis was used to estimate the contribution of N sources in groundwater from three end-members (i.e., rainwater, natural snow, and artificial snow).

https://doi.org/10.5194/egusphere-2025-190
Preprint. Discussion started: 7 March 2025


## 3 Results and discussion

### 3.1 Snowmelt period

Figure 3a shows the monthly precipitation and temperature trends, with the highest precipitation (330 mm) in August and the lowest (3 mm) in February, alongside summer and winter temperature extremes of +30.8°C and −23.4°C, respectively. Figure 3b shows snowfall periods from December 2, 2020, to March 7, 2021, and from November 2021 to April 1, 2022, coinciding with sub-zero atmospheric temperatures. Although the snowfall at the mountain summit could not be measured, the existence of snow cover could be inferred from the soil temperature. Because snow acts as an insulator, the soil temperature under the snowpack is maintained at 0°C. Therefore, the soil temperature was kept constant at 0°C from late February to mid-May 2021 and from early March to early May 2022, indicating that snow cover existed during that period (Figure 3b). When snowmelt infiltration started in late February 2021 and early March 2022, the soil moisture content showed a wide variation, ranging from 0.1 to 0.45 $m^3/m^3$ (Figure 3c). However, soil moisture content showed frequent variation within a narrow range of 0.3 to 0.5 $m^3/m^3$ as the snow cover disappeared after May 2021 and May 2022. The infiltrated snowmelt water percolates into the surrounding groundwater or contributes to surface runoff, eventually entering rivers and impacting their water quality (Lee et al., 2008). In fact, the snowmelt event affected the water level and water quality in the surrounding stream (Songcheon) within the study area (Figure 3d). $NO_3^-$–N concentrations decreased when snowmelt began in late February, coinciding with rising water levels. A similar pattern occurs during the summer monsoon season.

### 3.2 Origin of water

In high mountain areas, groundwater recharge primarily occurs through precipitation, including rainfall and the melting of snow (Somers and McKenzie, 2020). Therefore, understanding the stable water isotopes ($\delta^{18}O$–$H_2O$ and $\delta^2H$–$H_2O$) in precipitation, which is the primary water source to catchments, is important for better understanding the hydrologic cycle (Ingraham, 1998). In this study, $\delta^{18}O$–$H_2O$ and $\delta^2H$–$H_2O$ values of the spring/summer rainfall ($n = 4$) ranged from −13.97‰ to −10.48‰ (−11.91 ± 1.47‰, 1σ) and from −96.70‰ to −75.58‰ (−82.84 ± 9.57‰, 1σ), respectively (Table S3). In particular, $\delta^{18}O$–$H_2O$ and $\delta^2H$–$H_2O$ values of precipitation were further depleted by 1.87‰ and 12.59‰, respectively, at high altitude (1,420 m) relative to low altitude (770 m) due to "amount effect" (Siegenthaler and Oeschger, 1980). Meanwhile, the $\delta^{18}O$–$H_2O$ and $\delta^2H$–$H_2O$ of natural snow ($n = 4$), with the exception of the top of the sublimation layer, ranged from −13.94‰ to −11.46‰ (−12.71 ± 1.01‰, 1σ) and from −89.23‰ to −63.51‰ (−80.69 ± 12.02‰, 1σ), respectively. Winter precipitation from cold regions has more depleted stable isotope values because lower cloud condensation temperatures lead to higher fractionation factors (Dansgaard, 1964).

On the $\delta^{18}O$ vs. $\delta^2H$ diagram, most samples, excluding certain snow samples, are positioned directly on or near the LMWL ($\delta^2H = 8.18 \times \delta^{18}O + 14.66$; $R^2 = 0.80$) with slopes consistent with the best fit lines (Figure 4a). Samples from the bottom layer of natural snow are plotted away from the LMWL, indicating that isotopic exchange between the liquid water and ice inside the snow during melting may have occurred before and/or during hydrological processes and transport (Lee et al., 2010a; Lee

https://doi.org/10.5194/egusphere-2025-190
Preprint. Discussion started: 7 March 2025


et al., 2010b). Meanwhile, the linear trend of groundwater (YP) under the mountain ($\delta^2H = 6.43 \times \delta^{18}O - 3.35$, $R^2 = 0.95$, $n$ = 32) and artificial snow samples plotted under the LMWL, as well as the lower slope, suggests that the sampled water underwent evaporative loss (Dansgaard, 1964; Lee et al., 2010b; Jung et al., 2021). The $\delta^{18}O$–$H_2O$ and $\delta^2H$–$H_2O$ values of surface water ($n$ = 5) ranged from −10.04‰ to −9.32‰ (−9.76 ± 0.30‰, 1σ) and from −67.32‰ to −61.35‰ (−64.91 ± 2.49‰, 1σ), respectively, and these samples were similar in isotopic composition to artificial snow samples ($n$ = 2; −9.08 ± 0.17‰, 1σ for $\delta^{18}O$–$H_2O$ and −63.30 ± 1.44‰, 1σ for $\delta^2H$–$H_2O$). The $\delta^{18}O$–$H_2O$ and $\delta^2H$–$H_2O$ of mountain groundwater (W, $n$ = 12) ranged from −10.76‰ to −10.53‰ (−10.65 ± 0.08‰, 1σ) and from −71.65‰ to −69.58‰ (−70.67 ± 0.65‰, 1σ), respectively, between precipitation and artificial snow/surface water samples. These observations suggest that the mountain groundwater (W) in the study area is a mixture of precipitation and artificial snow. In addition, the stable water isotopes of mountain groundwater (W) showed a lower value than those of groundwater (YP) under the mountain, which reflects the depleted isotope values and precipitation at high altitudes.

### 3.3 Sources of nitrate

Typical values of $\delta^{15}N$ and $\delta^{18}O$ of nitrate derived or nitrified from various N sources are summarized in Table S4. In this study, the $\delta^{15}N$–$NO_3^-$ and $\delta^{18}O$–$NO_3^-$ values of atmospheric deposition (snow and rainfall; $n$ = 5) ranged from +2.12‰ to +8.34‰ and from +17.87‰ to +86.09‰, respectively (Figure 4b; Table S3). The highest $\delta^{15}N$–$NO_3^-$ value (+8.34‰) was observed during winter rainfall (February 2021), and the lowest $\delta^{15}N$–$NO_3^-$ value (+2.12‰) was observed during summer rainfall (August 2021). Low summer $\delta^{15}N$–$NO_3^-$ values may result from depleted $\delta^{15}N$–$NO_x$ causing increased biogenic soil emissions (including nitrification of fertilizers) and lightning during warmer months, and the enriched $\delta^{15}N$–$NO_x$ during colder seasons can be attributed to the increased combustion of fossil fuels (Freyer, 1978; Zhang et al., 2003; Jaegle et al., 2005).

Meanwhile, $\delta^{18}O$–$NO_3^-$ is influenced by nitrate ($NO_3^-$) formation pathways and the associated isotopic fractionation, rather than by NOx sources (Hastings et al., 2003). The isotopic composition of artificial snow samples ($n$ = 2) was relatively high for $\delta^{15}N$–$NO_3^-$ (+9.88‰ and +10.69‰) and low for $\delta^{18}O$–$NO_3^-$ (+1.89‰ and +3.39‰), indicating a manure/sewage source. The $\delta^{15}N$–$NO_3^-$ and $\delta^{18}O$–$NO_3^-$ of the surface water ($n$ = 5) ranged from 7.99‰ to 12.84‰ (9.76 ± 1.92‰, 1σ) and from 0.54‰ to 3.43‰ (1.60 ± 1.27‰, 1σ), respectively. The isotope values of the artificial snow were similar to those of surface water, suggesting that surface water was used to make artificial snow. The $\delta^{15}N$–$NO_3^-$ and $\delta^{18}O$–$NO_3^-$ of mountain groundwater (W, $n$ = 12) ranged from 6.45‰ to 7.77‰ (6.98 ± 0.37‰, 1σ) and from −1.69‰ to 8.47‰ (2.40 ± 2.29‰, 1σ), respectively, overlapping with the range of soil N and manure/sewage sources.

We additionally collected $NO_3^-$ concentration data of mountain groundwater (W) from previous reports to investigate how N sources varied seasonally from 2018 to 2022 (Hanil Tech Co., Ltd, 2018; Hanil Tech Co., Ltd, 2019; KIGAM, 2020). Figure 5a shows the temporal variation in the average $NO_3^-$–N concentration from the W1 and W2 wells along with their isotope values. The $NO_3^-$–N concentration showed substantial seasonal variations ($p$ = 0.05, one-tailed t-test), with a higher concentration observed during the dry season (December, January, and February) relative to the wet season (July, August, and September). This pattern could be due to the dilution effect caused by heavy rainfall during the wet season. As mentioned

https://doi.org/10.5194/egusphere-2025-190
Preprint. Discussion started: 7 March 2025


previously, the $NO_3^-$–N concentration of stream water tended to decrease due to the dilution effect during the snowmelt period (March to May) and wet season (Figure 3d). However, $NO_3^-$–N concentrations in mountain groundwater (W) decreased only during the wet season; during snowmelt (May 2021), these concentrations were maintained at 4.52 mg/L, resembling the 4.49 mg/L concentrations recorded in the dry season (February 2021). This result suggests that the N source with a relatively high $NO_3^-$ concentration is continuously flowing into the mountain groundwater (W) along with natural snow.

In order to more accurately identify N sources, an understanding of stable water and nitrate isotopes is required. The $\delta^{15}N$–$NO_3^-$ value increased from 6.83‰ to 7.53‰ during the snowmelt period (Figure 5a), indicating input of a relatively enriched $^{15}N$ source such as manure/sewage (Figure 5b). Since agricultural activities and sewage discharge are absent on the mountain summit, the consistent $NO_3^-$ concentrations and the increase in $\delta^{15}N$–$NO_3^-$ observed during the snowmelt period are likely attributed to the presence of artificial snow. In contrast, when the $NO_3^-$ concentration decreased during the wet season, the $\delta^{15}N$–$NO_3^-$ isotope value decreased concurrently, likely due to the input of soil N with a relatively depleted $\delta^{15}N$–$NO_3^-$ isotope value. Beyond the current study area, the Baihepu Reservoir—used as a water source for artificial snow during the Beijing Olympics in China—showed the average $\delta^{15}N$–$NO_3^-$ isotope value of 9.69‰ in September 2012, December 2012 and June 2013, indicating M&S source (Li et al., 2014). Thus, if the water from the area were used to produce artificial snow, it could potentially introduce pollutants as well.

### 3.4 Quantifying the contribution of artificial snow to groundwater

Tracing N sources using only stable nitrate isotopes can limit accurate identification, as the isotopic ranges of different contaminants can overlap. As shown earlier, $\delta^{18}O$–$NO_3^-$ has been useful in separating atmospheric and microbial sources of nitrate, but the $\delta^{18}O$–$NO_3^-$ values of nitrification from $NH_4^+$ of fertilizer/precipitation, soil $NH_4^+$, and manure/sewage overlap (Figure 5b). In contrast, $\delta^{18}O$–$H_2O$ values from rainwater, natural snow, and artificial snow showed relatively distinct isotopic signatures (Figure 4a). In addition, analyses of stable water isotopes are not limited by minimum concentrations, so data can be obtained from even low-ion concentration samples such as precipitation. Since the late 1960s, hydrograph separation using stable water isotope tracers has resulted in major advances in catchment hydrology (Hubert et al., 1969; Mook et al., 1974; Fritz et al., 1976; Sklash et al., 1976; Hermann et al., 1978; Klaus and McDonnell, 2013). Therefore, the use of $\delta^{18}O$–$H_2O$ in combination with $\delta^{15}N$–$NO_3^-$ may improve the reliability of N source identification (Li et al., 2010; Yue et al., 2004; Lingle et al., 2017).

To identify the predominant N sources in mountain groundwater (W), we estimated the contribution of N sources using Bayesian mixing models. In the bivariate mixing diagram shown in Figure 6a, the cluster of values representing mountain groundwater (W) samples lies within the mixing area of the three end-members (rainwater, natural snow and artificial snow). Isotopic compositions of end-members are defined in Table S5. Rainwater and natural snow samples, collected from the mountain summit in August 2022 and in February 2021 and May 2021, respectively, were used. As mentioned above, water isotope values of the top layer of natural snow were excluded from the data set due to sublimation. In addition, samples with $NO_3^-$ concentrations below the detection limit (< 0.037 mg/L for $NO_3$) or with generally low $NO_3^-$ concentrations (< 0.5 mg/L)

https://doi.org/10.5194/egusphere-2025-190
Preprint. Discussion started: 7 March 2025


were unavoidably excluded due to difficulty in analyzing nitrate isotopes or issues with low accuracy. The average N contribution was highest in artificial snow (49.5%), followed by rainwater (31.6%) and natural snow (18.7%) (Figure 6b), and artificial snow was a dominant N source.

We estimated the theoretical nitrate-N loading ratio in groundwater using end-member mixing model based on related parameters (Table 1) and compared it with the average N contribution. The N input from rainwater and natural snow was determined by accounting for the average $NO_3^-$-N concentration of each end-member obtained in this study, annual water usage for snowmaking, precipitation, and the watershed area. According to Lee and Kim (2007), groundwater recharge in the upper North Han River basin, where the study area is included, exhibits seasonality with wet and dry seasons each accounting for approximately half a fraction. Consequently, this study calculated the ratio of dry/wet recharge rate by partitioning the contributions from summer and other precipitation, applying these proportions to the final calculation. The ratio of dry/wet recharge rate was 2.12, indicating a notably higher recharge during the dry season, attributed to increased recharge efficiency and reduced evapotranspiration (Winograd et al., 1998; Jasechko et al., 2014). As a result, the theoretical nitrate-N load ratio ranked as follows: rainwater (36.3%) > artificial snow (49.2%) > natural snow (14.5%). These results are closely consistent with previously calculated contributions (Figure 6b), highlighting the potential for artificial snow to contribute to long-term N accumulation in alpine ecosystems.

The N accumulated in this way undergoes denitrification by soil bacteria, resulting in N loss and the potential release of $N_2O$ greenhouse gas, which affects soil N availability and contributes to climate change. This underscores the dual environmental impact of artificial snow on N cycling and greenhouse gas emissions, reinforcing the need to monitor N dynamics in ecosystems affected by artificial snow. In fact, the main global source of $N_2O$ is microbial production in soils, and N inputs from atmospheric deposition caused 51% of anthropogenic $N_2O$ emissions from soils in 2020 (Erisman et al., 2013). The greenhouse gas emissions will exacerbate global warming, thereby fueling a cycle that further amplifies the need for artificial snow production. This feedback loop highlights a paradox where the activities intended to mitigate the effects of climate change in winter tourism may, in turn, contribute to the broader issue of global warming. As global warming progresses, the need for artificial snow is expected to increase further than now. These persistent N source inputs can significantly impact N cycling, making long-term monitoring of their impacts crucial.

## 4 Conclusions

We demonstrated the influence of N sources in artificial snow on the surrounding groundwater of a ski resort. Snowmaking requires large amounts of electricity, and generating this electricity requires the use of fossil fuels, which emit greenhouse gases such as carbon dioxide ($CO_2$). Greenhouse gas emissions from artificial snow production will accelerate further warming of the climate, in turn requiring more artificial snow and creating a positive feedback loop. In addition, denitrification reactions by soil bacteria occur as artificial snow is distributed over the soil, and the emission of nitrous oxide ($N_2O$) gas, which is a product of denitrification, can further intensify global warming. As a result, these anthropogenic N inputs could have important implications for nitrogen cycling. Therefore, long-term monitoring of these impacts is essential, as the use of artificial snow will continue to increase due to climate change.

**Author contributions**

HJ: conceptualization, data curation, formal analysis, visualization, writing (original draft). YN: conceptualization, funding acquisition, validation, resources, writing (review). KK: funding acquisition, data curation, resources, writing (review and editing). DK: funding acquisition. WK: writing (review and editing). JL: conceptualization, methodology, validation, funding acquisition, writing (review and editing).

**Competing interests**

The contact author has declared that none of the authors has any competing interests.

**Acknowledgements**

This study was supported by a National Research Foundation of Korea (NRF) grant funded by the Korean government (MSIT, NRF-2022R1A2C3007047) and a research grant by a National Research Council of Science and Technology grant from the Korean government (CAP-17-05-KIGAM). Additional partial support was provided by the Korea Environment Industry & Technology Institute (KEITI) through Aquatic Ecosystem Conservation Research Program, funded by the Korea Ministry of Environment (MOE) (RS-2024-00332851).

https://doi.org/10.5194/egusphere-2025-190
Preprint. Discussion started: 7 March 2025


**Table 1**
Parameters and values for the quantification of discharge rate from17/18 to 23/24 season.

| Parameters | Values | Reference |
|---|---|---|
| Annual precipitation (mm) | 1324.2 (Summer: 899.2) | Korea Meteorological Administration (KMA) |
| Watershed area ($m^2$) | 5,800,509 | Hanil Tech Co., Ltd. (2019) |
| Annual water usage for snowmaking ($m^3$) | 1,067,082 | Yongpyong ski resort |
| Ratio of recharge rate (Dry season/Wet season) | 2.12 | Calculated |

https://doi.org/10.5194/egusphere-2025-190
Preprint. Discussion started: 7 March 2025


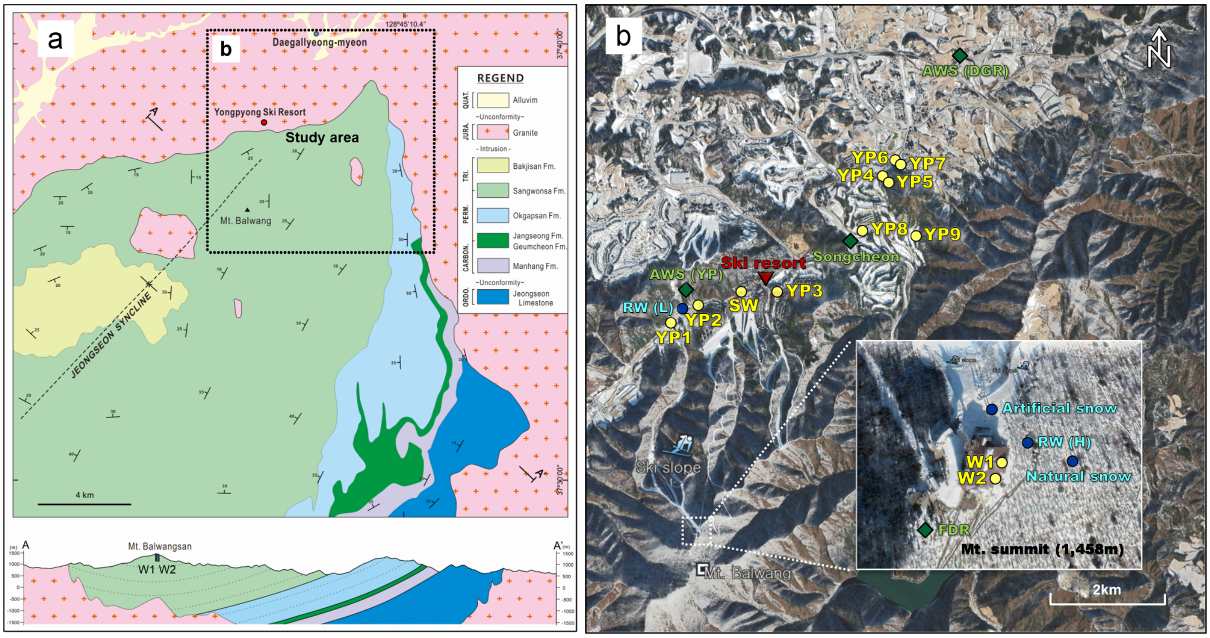


**Figure 1.** (a) Geological map and transverse cross-section of Mt. Balwang and surrounding areas, South Korea. (b) Location of the sampling and monitoring sites (modified Landsat images from December 2022 acquired from © Google Earth). The ski slopes start at the mountain summit at a 1,458-m altitude and continue down to 700 m below the mountain (ski resort). Stream water (SW) was collected from the stream at the entrance of the ski resort. Groundwater (GW) samples were collected on the mountain summit (W1 and W2) and under the mountain (YP1–YP9). Rainwater (RW) samples were also collected on the mountain summit (RW [H]) and under the mountain (RW [L]). The automatic weather stations (AWS; Yongpyong [YP] and Daegwangryeong [DGR]) and stream water quality monitoring sites (Songcheon) surrounding the ski resort. Soil moisture content and soil temperature were measured using frequency domain reflectometry (FDR) sensors.

https://doi.org/10.5194/egusphere-2025-190
Preprint. Discussion started: 7 March 2025


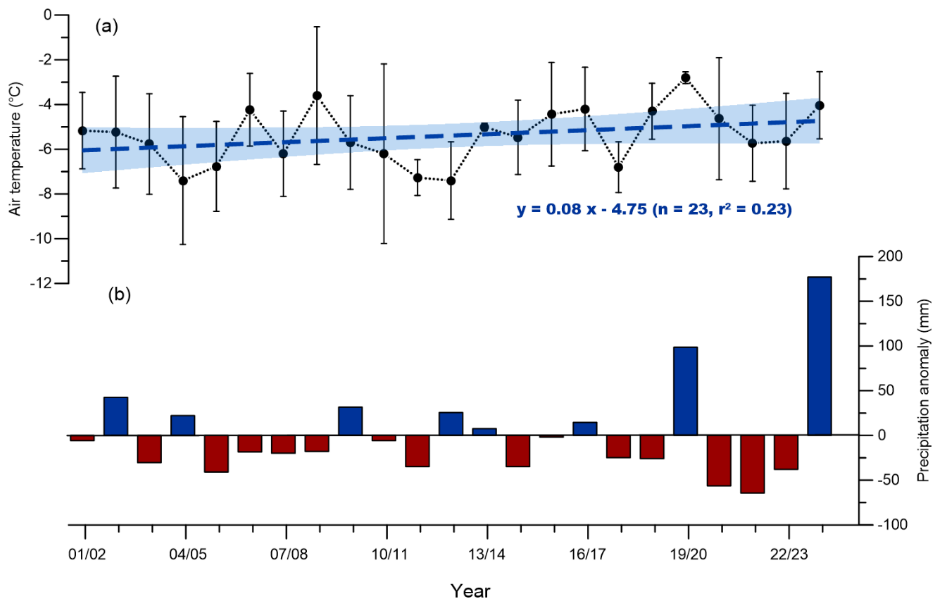


**Figure 2.** During the winter ski season (December-February) from 2001/2002 to 2023/2024, temporal variations of (a) average air temperature (with error bar representing standard deviation) and (b) precipitation anomaly in Yongpyeong. The blue dotted line and the blue shaded areas indicate the trend from linear regression for air temperature and the 95% confidence intervals, respectively.

https://doi.org/10.5194/egusphere-2025-190
Preprint. Discussion started: 7 March 2025


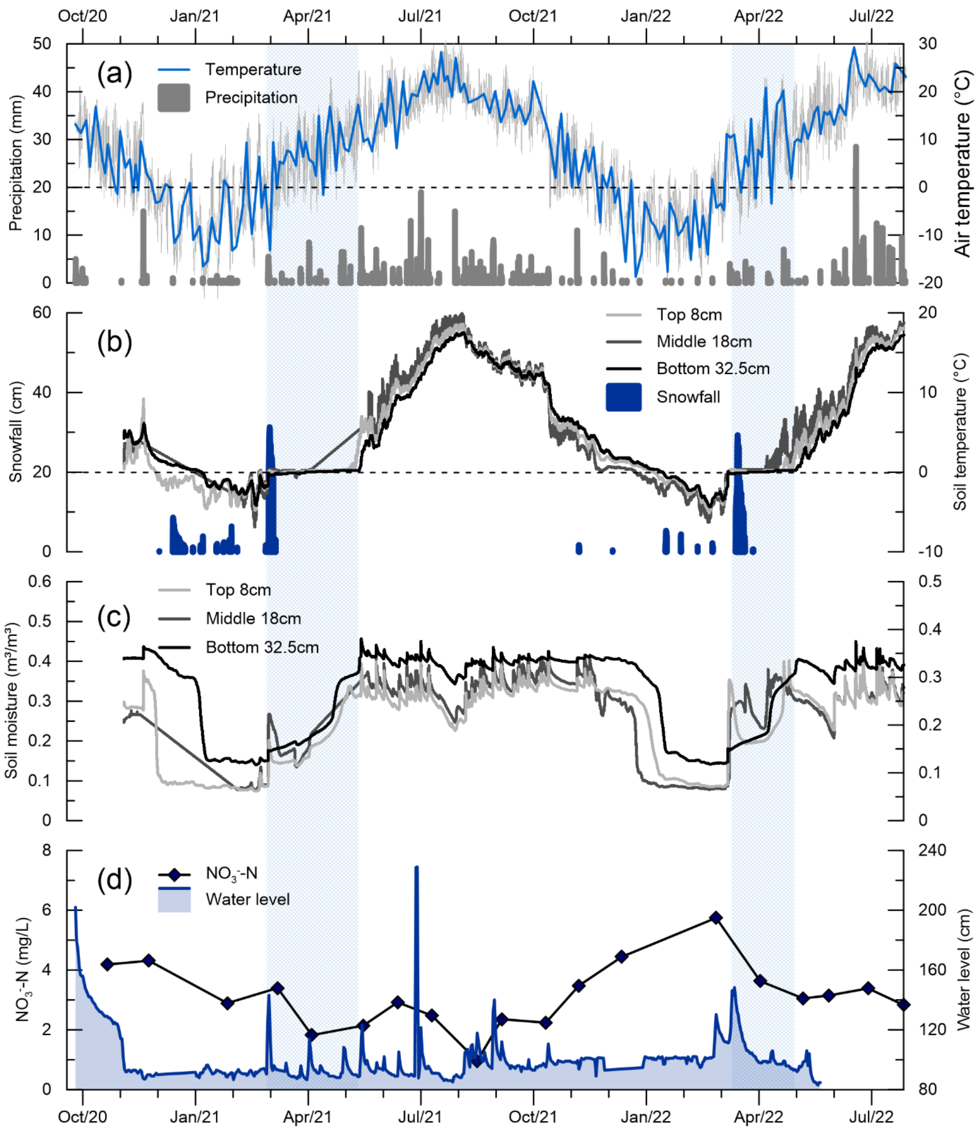


Figure 3. (a) Temporal variation in precipitation and air temperature data from the automatic weather station (Yongpyong). (b) Soil temperature in comparison with snowfall from the automatic weather station (Daegwallyeong). (c) Soil moisture content. (d) $NO_3^-$–N concentrations and water level monitoring data from stream water used to make artificial snow.

https://doi.org/10.5194/egusphere-2025-190
Preprint. Discussion started: 7 March 2025


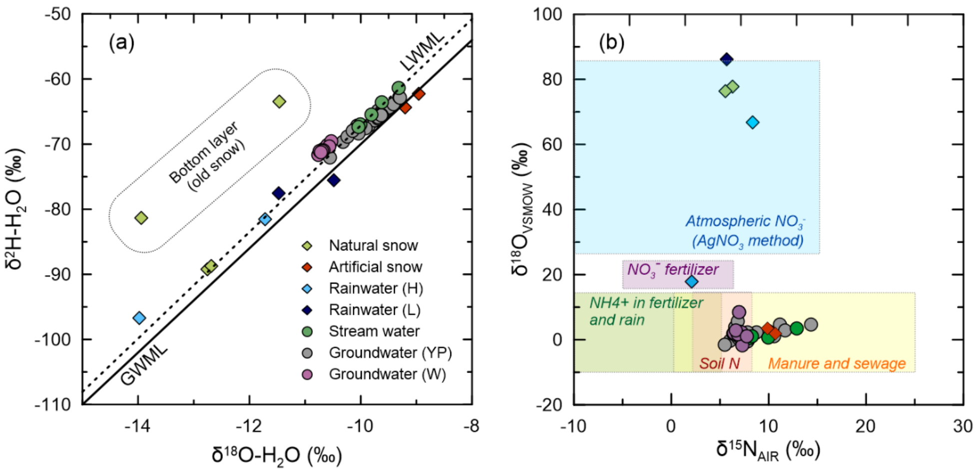


**Figure 4.** (a) Stable isotopic compositions ($\delta^2H$–$H_2O$ vs. $\delta^{18}O$–$H_2O$, ‰) for samples analyzed in this work alongside the global meteoric water line (GMWL; $\delta^2H = 8 \times \delta^{18}O + 10$, Craig [1961]) and the local meteoric water line (LMWL; $\delta^2H = 8.18 \times \delta^{18}O + 14.66$, Jung et al. [2023]) derived from the IAEA station in South Korea. (b) Nitrate isotopic compositions ($\delta^{18}O$–$NO_3$ vs. $\delta^{15}N$–$NO_3$, ‰) of various N sources (Kendall et al. [1998]) and isotopic values for samples obtained in our study.

https://doi.org/10.5194/egusphere-2025-190
Preprint. Discussion started: 7 March 2025


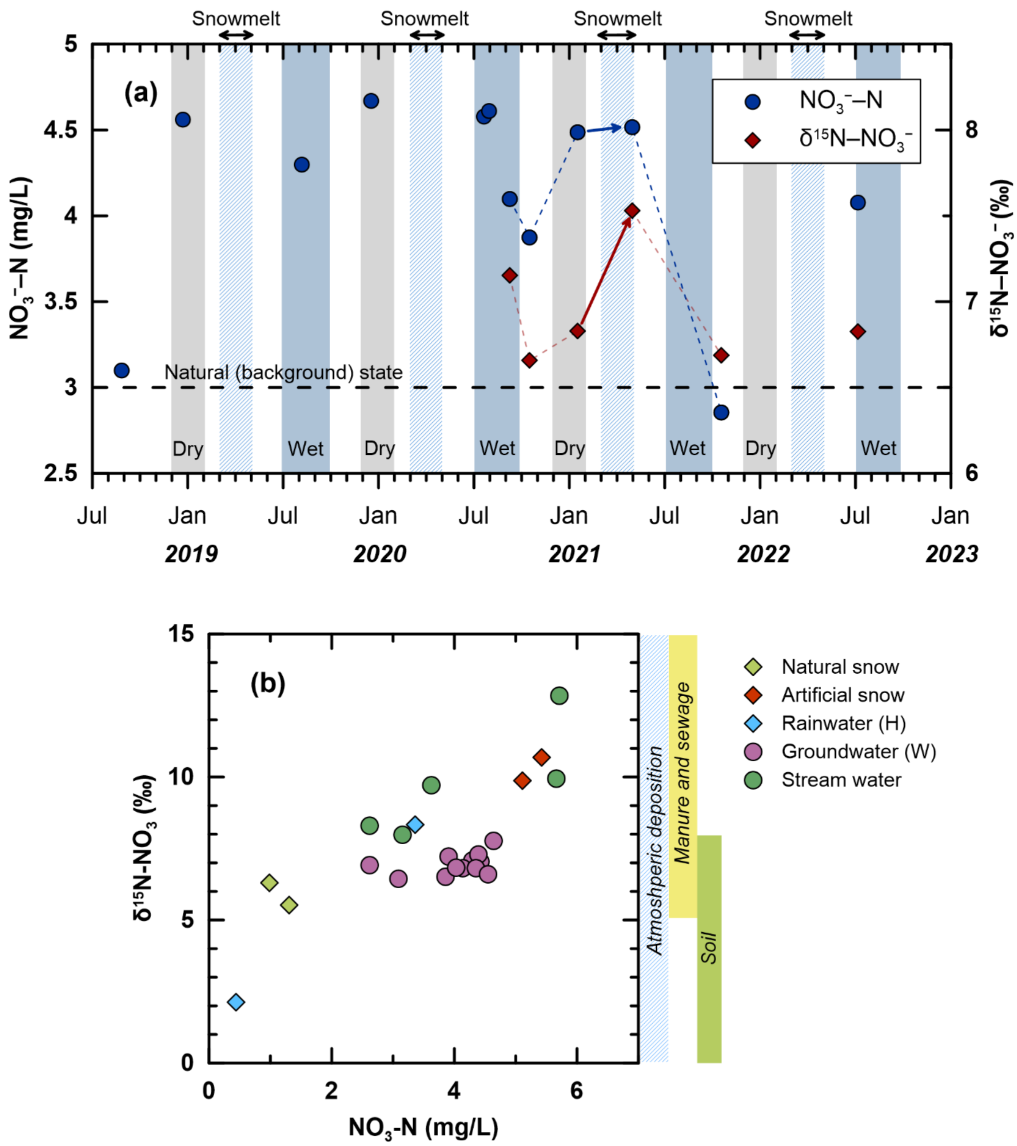


**Figure 5.** (a) Seasonal variation in N sources in mountain groundwater from 2018 to 2022. (b) Relationship between $\delta^{15}N$–$NO_3$ and $NO_3^-$–N concentrations of potential N sources for mountain groundwater.

https://doi.org/10.5194/egusphere-2025-190
Preprint. Discussion started: 7 March 2025


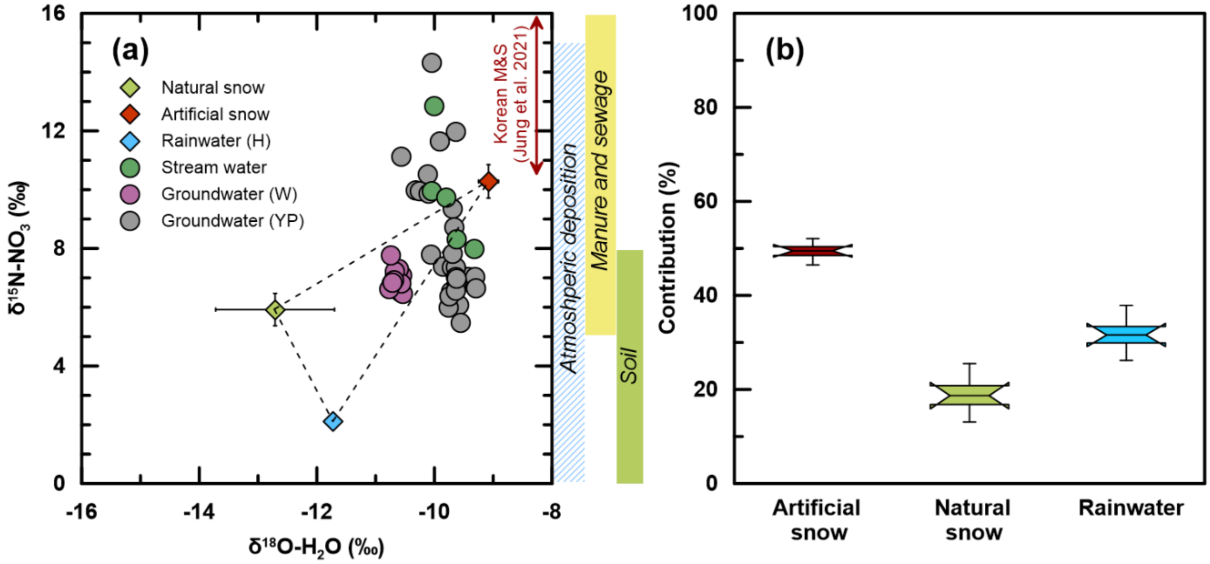


**Figure 6.** (a) Mixing diagram using δ$^{15}$N–$NO_3$ and δ$^{18}$O–$H_2O$. The line indicated by "Korean M&S" represents manure and sewage in Korea (Jung et al., 2021). The mean and standard deviation are shown for natural snow and artificial snow. (b) Boxplots showing the median and 25th and 75th percentile values (box extent) along with the 2.5th and 97.5th percentile values (whisker extent) of the contribution (%) of three potential N sources (artificial snow, natural snow, and rainwater) to mountain groundwater.

https://doi.org/10.5194/egusphere-2025-190
Preprint. Discussion started: 7 March 2025


## References

Craig, H. (1961). Isotopic Variations in Meteoric Waters. Science 133, 1702–1703.

Damm, A., Köberl, J., and Prettenthaler, F. (2014). Does artificial snow production pay under future climate conditions?–A case study for a vulnerable ski area in Austria. Tourism management 43, 8–21.

Dansgaard, W. (1964). Stable isotopes in precipitation. Tellus 16, 436–468.

Erisman, J.W., Galloway, J.N., Seitzinger, S., Bleeker, A., Dise, N.B., Petrescu, A.M.R., Leach, A.M., and de Vries, W. (2013). Consequences of human modification of the global nitrogen cycle. Philosophical Transactions of the Royal Society B: Biological Sciences, 368(1621).

Freyer, H.D. (1978). Seasonal trends of $NH_4^+$ and $NO_3^-$ nitrogen isotope composition in rain collected at Julich, Germany. Tellus 30, 83−92.

Fritz, P., Cherry, J., Weyer, K. and Sklash, M. (1976). Storm runoff analyses using environmental isotopes and major ions Interpretation of Environmental Isotope and Hydrochemical Data in Groundwater, Panel Proceedings Series-International Atomic Energy Agency, International Atomic Energy Agency, Vienna, Austria, 111–130.

Galloway, J.N., Aber, J.D., Erisman, J.W., Seitzinger, S.P., Howarth, R.W., Cowling, E.B., and Cosby, B.J. (2003). The nitrogen cascade. Bioscience, 53(4), 341-356.

Galloway, J.N., Schlesinger, W.H., Levy, H., Michaels, A., and Schnoor, J.L. (1995). Nitrogen fixation: Anthropogenic enhancement-environmental response. Global biogeochemical cycles 9, 235–252.

Hanil Tech Co., Ltd., (2018). Yongpyong Resort groundwater (W1) Development, Use, Groundwater impact investigation Report.

Hanil Tech Co., Ltd., (2019). Yongpyong Resort Groundwater (W2) Development Permission Groundwater Impact Investigation Report.

Hastings, M.G., Sigman, D.M. and Lipschultz, F. (2003). Isotopic evidence for source changes of nitrate in rain at Bermuda. Journal of Geophysical Research: Atmospheres 108, D24.

Hermann, A., Martinec, J. and Stichler, W. (1978). Study of snowmelt-runoff components using isotope measurements S.C. Colbeck, M. Ray (Eds.), Modeling of Snow Cover Runoff, U.S. Army Cold Regions Research and Engineering Laboratory, Hanover, NH.

Hubert, P., Marin, E., Meybeck, M., Olive, P., and Siwertz, E. (1969). Aspects Hydrologique, Gèochimique et Sèdimentologique de la Crue Exceptionnelle de la Dranse du Chablais du 22 Septembre 1968. Archives des Sciences 22, 581–604.

Ingraham, N.L. Isotopic variation in precipitation, in Isotope Tracers in Catchment Hydrology (eds. Kendall, C. and McDonnell, J.J.) 87–118 (Elsevier, Amsterdam, The Netherlands, 1998).

International Olympic Committee (IOC). (2022). Snow, climate change and the Olympic Winter Games. https://olympics.com/ioc/news/snow-climate-change-and-the-olympic-winter-games/

Jaegle, L., Steinberger, L., Martin, R.V. and Chance,K. (2005). Global partitioning of $NO_x$ sources using satellite observations: Relative roles of fossil fuel combustion, biomass burning, and soil emissions. Faraday Discuss. 130, 407−423.

Jasechko, S., Birks, S.J., Gleeson, T., Wada, Y., Fawcett, P.J. et al. (2014). The pronounced seasonality of global groundwater recharge. Water Resources Research, 50(11), 8845-8867.

https://doi.org/10.5194/egusphere-2025-190
Preprint. Discussion started: 7 March 2025


Jung, H., Kim, Y.S., Yoo, J., Han, S.J., and Lee, J. (2023). Identification of nitrate sources in tap water sources across South Korea using multiple stable isotopes: Implications for land use and water management. Science of the Total Environment 864.

Jung, H., Kim, Y.S., Yoo, J., Park, B., and Lee, J. (2021). Seasonal variations in stable nitrate isotopes combined with stable water isotopes in a wastewater treatment plant: implications for nitrogen sources and transformation. Journal of Hydrology 599, 126488.

Kendall, C. Tracing nitrogen sources and cycling in catchments, in Isotope Tracers in Catchment Hydrology (eds. Kendall, C. and McDonnell, J.J.) 519–576 (Elsevier, Amsterdam, The Netherlands, 1998).

Klaus, J. and Mc Donnell, J.J. (2013). Hydrograph separation using stable isotopes: Review and evaluation. Journal of hydrology 505, 47–64.

Knowles, N., Scott, D., and Steiger, R. (2024). Sustainability of snowmaking as climate change (mal)adaptation: an assessment of water, energy, and emissions in Canada's ski industry. Current Issues in Tourism 27(10), 1613–1630.

Korea Institute of Geoscience and Mineral Resources (KIGAM). (2020). Mt. Balwang Groundwater Optimum Utilization Development, Utilization and Management Plan.

Lee, J., Feng, X., Faiia, A.M., Posmentier, E.S., Kirchner, J.W., Osterhuber, R., and Taylor, S. (2010a). Isotopic evolution of a seasonal snowcover and its melt by isotopic exchange between liquid water and ice. Chemical geology 270, 126–134.

Lee, J., Feng, X.H., Faiia, A., Posmentier, E., Osterhuber, R., and Kirchner, J. (2010b). Isotopic evolution of snowmelt: A new model incorporating mobile and immobile water. Water Resources Research 46, W11512.

Lee, J., Nez, V.E., Feng, X.H., Kirchner, J.W., Osterhuber, R., and Renshaw, C.E. (2008). A study of solute redistribution and transport in seasonal snowpack using natural and artificial tracers. Journal of Hydrology 357, 243–254.

Lee, K.S., & Kim, Y. (2007). Determining the seasonality of groundwater recharge using water isotopes: a case study from the upper North Han River basin, Korea. Environmental Geology, 52, 853-859.

Li, C., Jiang, Y.B., Guo, X.Y., Cao, Y., and Ji, H.B. (2014). Multi-isotope ($^{15}N$, $^{18}O$ and $^{13}C$) indicators of sources and fate of nitrate in the upper stream of Chaobai River, Beijing, China. Environmental Science: Processes & Impacts 16, 2644–2655.

Li, S.L., Liu, C.Q., Li, J., Liu, X., Chetelat, B., Wang, B., and Wang, F. (2010). Assessment of the sources of nitrate in the Changjiang River, China using a nitrogen and oxygen isotopic approach. Environmental Science & Technology 44, 1573–1578.

Lingle, D.A., Kehew, A.E., and Krishnamurthy, R.V. (2017). Use of nitrogen isotopes and other geochemical tools to evaluate the source of ammonium in a confined glacial drift aquifer, Ottawa County, Michigan, USA. Applied geochemistry 78, 334–342.

Madison, R.J. and Brunett, J.O. (1985). Overview of the occurrence of nitrate in ground water of the United States. In: National water summary 1984: Hydrologic events, selected water-quality trends, and ground-water resources. In: USGS Water Supply Pap, 2275. U.S. Gov. Print. Office, Washington, DC, pp. 93–105.

Mook, W., Groeneveld, D., Brown, A. and Van Ganswijk, A. (1974). Analysis of a runoff hydrograph by means of natural $^{18}O$. Isotope Techniques in Groundwater Hydrology, International Atomic Energy Agency, Vienna, 145–156.

Morin, S., François, H., Réveillet, M., Sauquet, E., Crochemore, L. et al. (2023). Simulated hydrological effects of grooming and snowmaking in a ski resort on the local water balance. Hydrology and Earth System Sciences, 27(23), 4257-4277.

Parnell, A.C. (2008). SIAR: Stable Isotope Analysis in R. R Package Version 3.

https://doi.org/10.5194/egusphere-2025-190
Preprint. Discussion started: 7 March 2025


Parnell, A.C. and Inger, R. (2016). Simmr: A Stable Isotope Mixing Model R Package Version 0.4.1.

Rixen, C., & Rolando, A. (2013). *The impacts of skiing and related winter recreational activities on mountain environments* (p. 236). Bentham Science Publishers.

Schlesinger, W. H. (2009). On the fate of anthropogenic nitrogen. Proceedings of the National Academy of Sciences 106, 203–208.

Siegenthaler, U. and Oeschger, H. (1980). Correlation of 18O in precipitation with temperature and altitude. Nature 285, 314–317.

Sklash, M.G., Farvolden, R.N. and Fritz, P. (1976). A conceptual model of watershed response to rainfall, developed through the use of oxygen-18 as a natural tracer. Canadian Journal of Earth Sciences 13, 271–283.

Somers, L.D. and McKenzie, J.M. (2020). A review of groundwater in high mountain environments. Wiley Interdisciplinary Reviews: Water 7, e1475.

Vorkauf, M., Steiger, R., Abegg, B., and Hiltbrunner, E. (2024). Snowmaking in a warmer climate: an in-depth analysis of future water demands for the ski resort Andermatt-Sedrun-Disentis (Switzerland) in the twenty-first century. International Journal of Biometeorology (2022).

Winograd, I.J., Riggs, A.C., & Coplen, T.B. (1998). The relative contributions of summer and cool-season precipitation to groundwater recharge, Spring Mountains, Nevada, USA. Hydrogeology journal, 6, 77-93.

Yue, F.J., Liu, C.Q., Li, S.L., Zhao, Z.Q., Liu, X.L., Ding, H., Liu, B.J., and Zhong, J. (2014). Analysis of $\delta^{15}N$ and $\delta^{18}O$ to identify nitrate sources and transformations in Songhua River, Northeast China. Journal of Hydrology 519, 329–339.

Zhang, R.Y., Tie, X.X. and Bond, D.W. (2003). Impacts of anthropogenic and natural $NO_x$ sources over the U.S. on tropospheric chemistry. Proceedings of the National Academy of Sciences 100, 1505−1509.